

pubs.acs.org/JACS Article

# Nanoparticle Superlattices through Template-Encoded DNA Dendrimers

Ho Fung Cheng,<sup>‡</sup> Max E. Distler,<sup>‡</sup> Byeongdu Lee, Wenjie Zhou, Steven Weigand, and Chad A. Mirkin\*



Cite This: J. Am. Chem. Soc. 2021, 143, 17170–17179



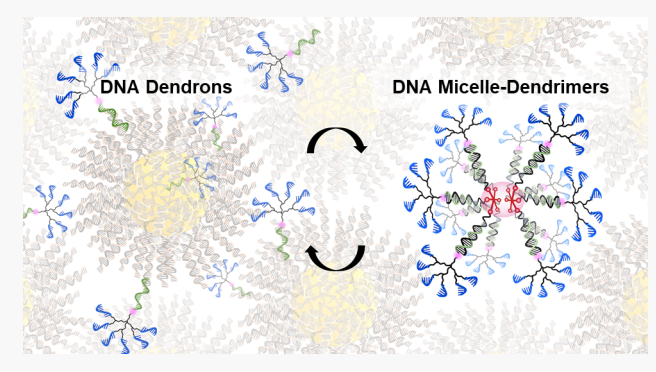
**ACCESS** 

Metrics & More



Supporting Information

ABSTRACT: The chemical interactions that lead to the emergence of hierarchical structures are often highly complex and difficult to program. Herein, the synthesis of a series of superlattices based upon 30 different structurally reconfigurable DNA dendrimers is reported, each of which presents a well-defined number of single-stranded oligonucleotides (i.e., sticky ends) on its surface. Such building blocks assemble with complementary DNA-functionalized gold nanoparticles (AuNPs) to yield five distinct crystal structures, depending upon choice of dendrimer and defined by phase symmetry. These DNA dendrimers can associate to form micelledendrimers, whereby the extent of association can be modulated based upon surfactant concentration and dendrimer length to produce a low-symmetry Ti<sub>5</sub>Ga<sub>4</sub>-type phase that has yet to be



reported in the field of colloidal crystal engineering. Taken together, colloidal crystals that feature three different types of particle bonding interactions—template—dendron, dendrimer—dendrimer, and DNA—modified AuNP-dendrimer—are reported, illustrating how sequence-defined recognition and dynamic association can be combined to yield complex hierarchical materials.

### INTRODUCTION

Biopolymers assemble into hierarchical structures through sequence-defined intra- and intermolecular interactions. The specificity of these interactions renders these macromolecules powerful building blocks for material design. Alternatively, many synthetic macromolecules, such as block copolymers, 1-4 dendrons, 5-8 or amphiphiles, 9-12 can undergo shape- or topology-controlled packing. These synthetic structures can associate with one another through dynamic, supramolecular interactions to yield nanoscale domains with adaptable sizes and shapes, 3-6,8,10,12 enabling the formation of hierarchical materials that have unconventional, low-symmetry phases. 2,3,5,6,10-12 Developing nanoscale building blocks that are capable of forming both dynamic associations and sequence-defined interactions (akin to those found in biology) could afford novel structure types and provide important insights into how hierarchical architectures arise in both natural and synthetic systems.

Various macromolecular architectures have been utilized to mediate the assembly of nanoparticle building blocks. <sup>13,14</sup> In particular, colloidal crystal engineering with DNA has emerged as a powerful, sequence-defined approach to program nanoparticle assembly, <sup>15</sup> with control over phase symmetries, lattice parameters, crystal habits, and thermostabilities. <sup>16–18</sup> In this approach, nanoparticles are functionalized with a dense shell of radially oriented oligonucleotides, which mediate interparticle bonding via sequence-specific complementary base-pairing. These DNA-functionalized nanoscale building blocks, also

known as programmable atom equivalents (PAEs),<sup>19</sup> are typically synthesized from nanoparticle cores that are structurally static. We hypothesized that by employing DNA-presenting supramolecules that can undergo dynamic structural reorganization, novel nanoparticle arrangements could be templated, and new lattice reconfiguration strategies could be enabled. We posited that such supramolecules should assemble through transient interactions that are orthogonal to the sequence-specific DNA hybridizations, which serve to direct the formation of nanoparticle superlattices.

Herein, we realized such supramolecular PAEs using a new type of DNA dendrimer composed of molecularly defined building blocks (Figure 1a). We co-assembled these dendrimers with gold nanoparticle (AuNP)-based PAEs (Figure 1b) and, by comprehensively screening the phase space, we identified five distinct crystal structures, one of which has no precedent in the field of colloidal crystal engineering. Our investigation of the nanoscale organization of these superlattices led to a serendipitous discovery: dendrimer PAEs that bear hydrophobic moieties at their core can undergo

Received: July 27, 2021 Published: October 11, 2021





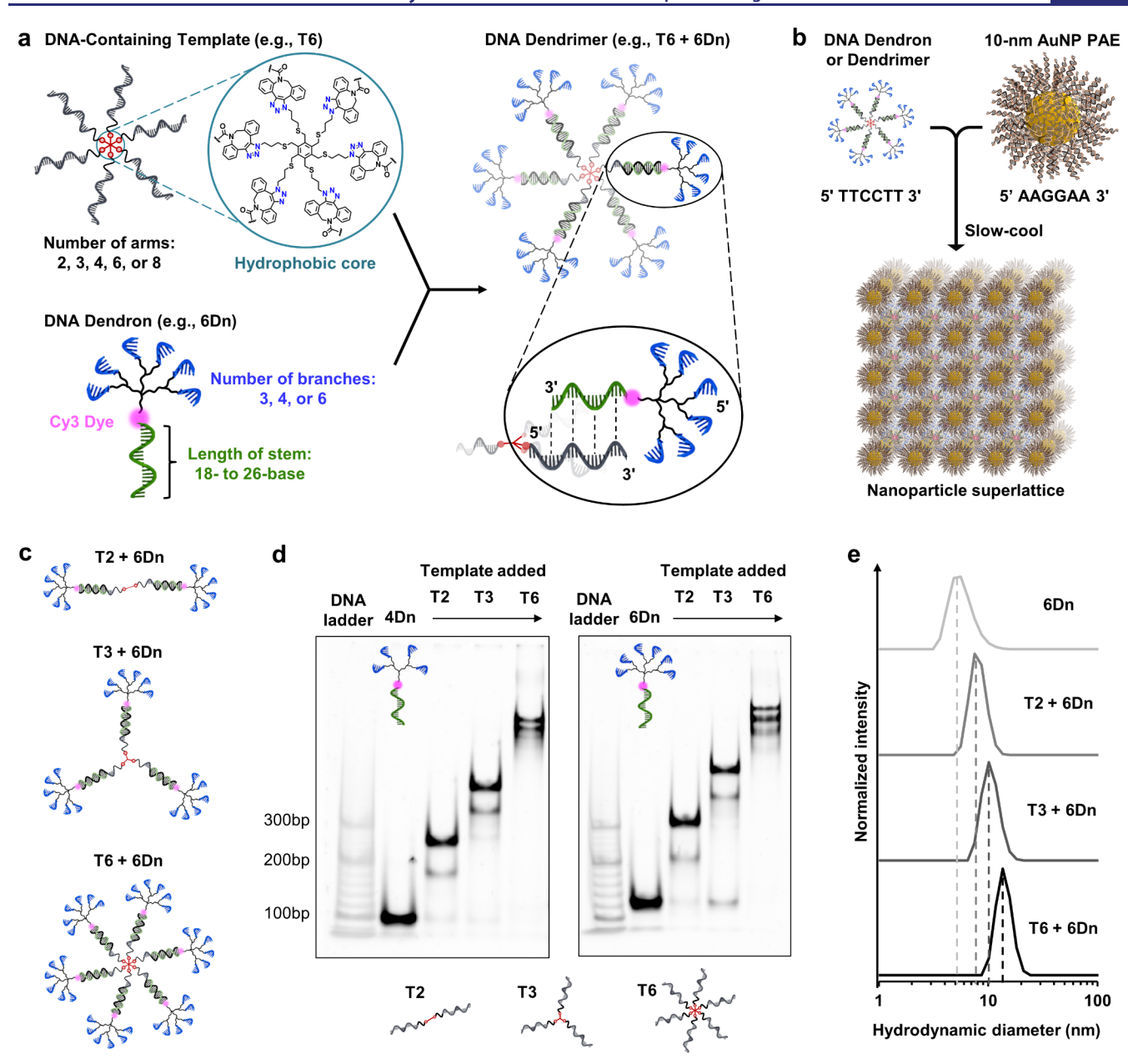


Figure 1. Bottom-up synthesis of supramolecular DNA dendrimers. (a) Left: DNA-containing templates have a hydrophobic core owing to the presence of dibenzocyclooctyne (DBCO) moieties. Depending on the structure of the molecular core, two to eight DNA strands can be installed (here, a six-arm DNA template is depicted). DNA dendrons can be synthesized with various branch numbers and stem lengths. Right: DNA dendrimers are assembled via hybridization between the template arms (black) and the dendron stems (green). (b) DNA dendrons or dendrimers were combined with 10 nm AuNP PAEs to form superlattices after slow-cooling. (c) A depiction of selected examples of DNA dendrimers. (d) Modular assembly of dendrons (4Dn and 6Dn) and templates (T2, T3, and T6) in 0.5 M NaCl results in defined DNA dendrimers that were characterized via 5% native polyacrylamide gel electrophoresis (PAGE). (e) Dynamic light scattering (DLS) shows that the hydrodynamic diameters ( $D_{\rm h}$ ) of these structures, dissolved in 0.5 M NaCl, 10 mM phosphate buffer, pH 7.4, increase with template valency. The dotted lines are there to guide the eye.

micelle-mediated association. The resulting colloidal crystals have three modes of organization: two that are programmed by DNA hybridization and one that is mediated by hydrophobic interactions. Each of these interactions can be toggled to control the assembly of these PAEs into various crystal structures.

# ■ RESULTS AND DISCUSSION

**Design and Synthesis of Supramolecular DNA Dendrimers.** Dendritic architectures are excellent nanoscale building blocks, 4,6,8 as they are molecularly precise, have a

defined topology, and can be heavily functionalized. Dendritic DNA, <sup>20,21</sup> developed for drug delivery and chemical sensing, <sup>22–25</sup> can be synthesized with a precise architecture by assembling a large number of oligonucleotides that have deliberately designed, orthogonal sequences. <sup>20,21,24,25</sup> To develop DNA dendrimers as a new type of building block in colloidal crystal engineering, we reasoned that our synthetic strategy should offer systematic, fine-tuned control over building block size, valency, and functionality.

Our approach to preparing DNA dendrimers (Figure 1a) uses two molecularly defined components (a template and a

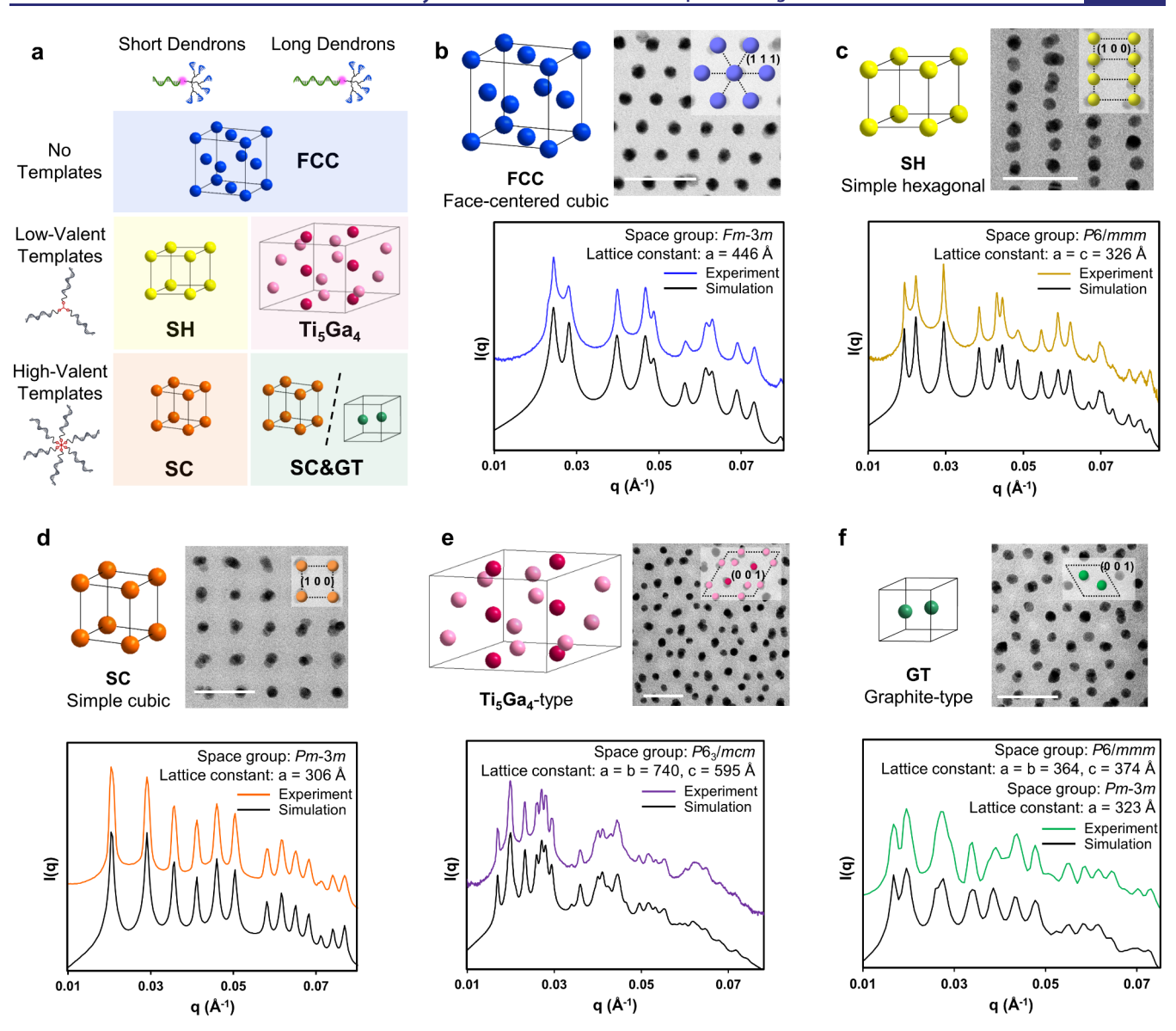


Figure 2. Superlattice phase symmetries and their characterization. (a) A depiction of the phase space: crystal structures depend on the presence and the identity of DNA-containing templates, as well as the stem length of the DNA dendrons (e.g., compared to 6Dn, 6Dn-L1 has an additional eight-base, non-hybridized region between the core and the branching region, while 6Dn-L2 and 6Dn-L3 have additional 12-base non-hybridized regions). (b–f) All structures were screened and characterized in the solution state via small-angle X-ray scattering (SAXS): (b) face-centered cubic (FCC), (c) simple hexagonal (SH), (d) simple cubic (SC), (e)  $Ti_5Ga_4$ -type, and (f) a mixture of graphite-type (GT) and SC. Colored traces are experimental data, and black traces are simulated spectra. Representative samples were imaged via scanning transmission electron microscopy (STEM) after stabilization in the solid state. Scale bars: 50 nm.

dendron) and one set of complementary DNA sequences. The DNA-containing templates were synthesized by conjugating multi-azide molecules with multiple copies of dibenzocyclooctyne (DBCO)-appended DNA,  $^{26,27}$  yielding constructs with a range of valences (Ta, the number of arms,  $a=2,\,3,\,4,\,6,\,$  or 8). Each arm possesses an 18- to 20-base sequence designed to hybridize to the stems of the DNA dendrons, with melting temperatures ( $T_{\rm m}$ ) greater than 60 °C under assembly conditions (Tables S1–S4). Each arm also has a six-base overhang that enables the resulting DNA dendrimer to be disassembled via toehold-mediated strand displacement (TMSD, vide infra).

Using various branching phosphoramidites,  $^{28,29}$  DNA dendrons were synthesized with three, four, or six branches (*b*Dn, the number of branches, b = 3, 4, or 6) (Figure 1a),  $^{30}$ 

each featuring single-stranded sticky ends (5' TTCCTT 3') that can hybridize with AuNP PAEs bearing complementary sticky ends (5' AAGGAA 3') (Figure 1b). The dendrons have an 18- to 26-base stem that hybridizes with the arms on a template, enabling one to control the distance between the branches and the dendrimer core. For example, the dendrons 6Dn, 6Dn-L1, 6Dn-L2, and 6Dn-L3 have incrementally longer stems (Table S3). A Cy3-phosphoramidite was incorporated in the stem to enable quantification of dendron content. All DNA architectures were purified using denaturing polyacrylamide gel electrophoresis (PAGE) and characterized using matrix-assisted laser desorption/ionization time-of-flight mass spectroscopy (MALDI-TOF MS) (Figures S1 and S2).

To establish that this hybridization-based approach can successfully produce supramolecular dendrimers (Figure 1c),

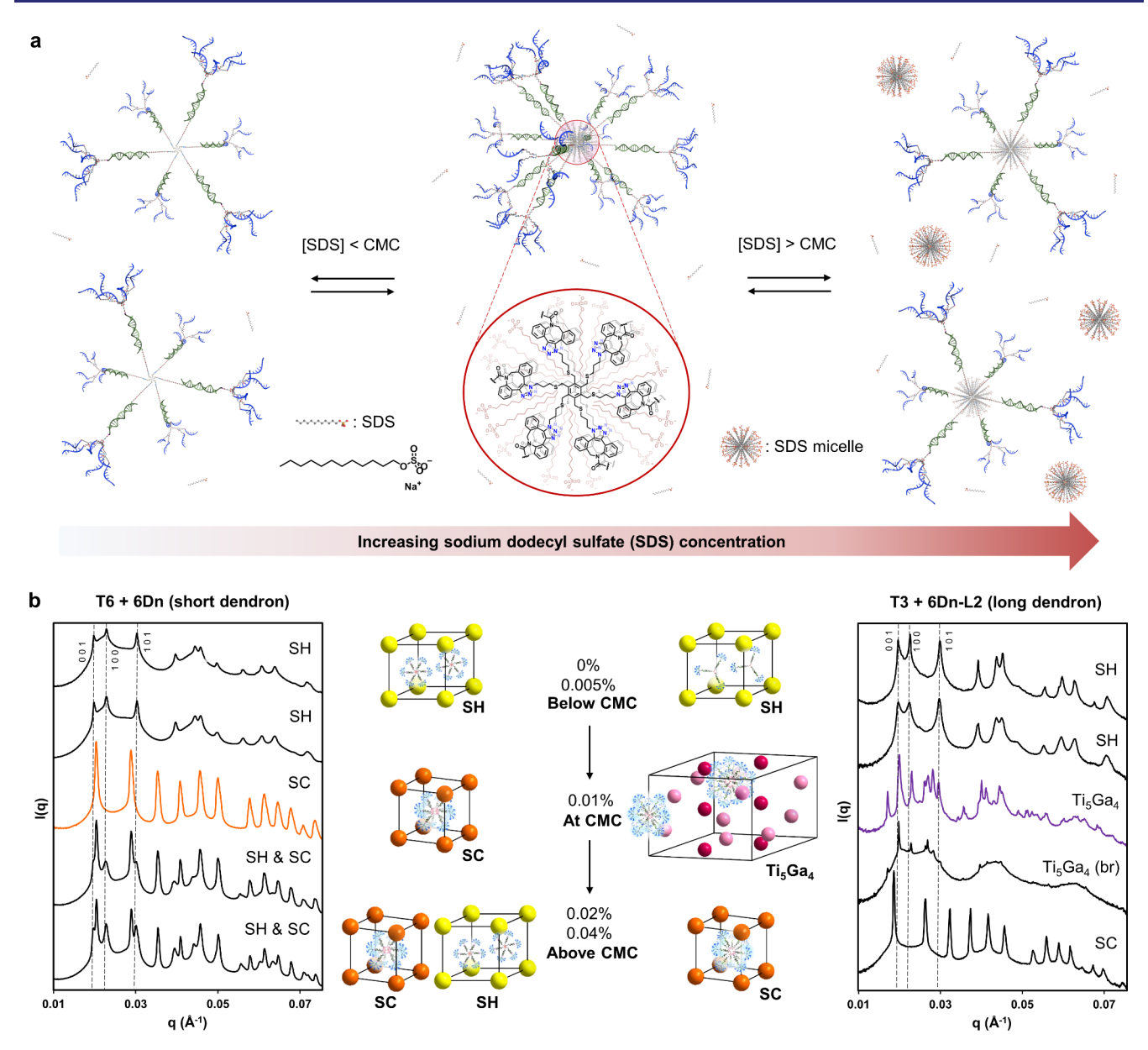


Figure 3. Surfactant-mediated DNA micelle-dendrimers. (a) Proposed pathway for dendrimer—dendrimer association. Surfactant sodium dodecyl sulfate (SDS) forms micelles at concentrations equal to or higher than the critical micelle concentration (CMC). These micelles encapsulate the hydrophobic cores of the templates, leading to dendrimer—dendrimer association at and slightly above the CMC. 3D models of DNA dendrimers and SDS micelles are drawn to scale. (b) From top to bottom: SAXS data collected at 0, 0.005, 0.01, 0.02, and 0.04% SDS. Left: T6 (0.1  $\mu$ M) and 6Dn (0.6  $\mu$ M). Right: T3 (0.2  $\mu$ M) and 6Dn-L2 (0.6  $\mu$ M), except for the sample at 0% SDS, whereby 1.5× concentrations were used to encourage aggregate formation. Center: observed crystal structures, represented by unit cells that depict DNA dendrimer and micelle-dendrimer locations. For clarity, not all micelle-dendrimers in the Ti<sub>5</sub>Ga<sub>4</sub>-type unit cell are drawn. Below the CMC, dendrimers do not associate with one another. At the CMC, the dendrimers associate to the greatest extent, significantly modulated by dendron stem length. Above the CMC, the dendrimers are distributed across a larger number of micelles, leading to less dendrimer—dendrimer association.

dendrons (4Dn and 6Dn), and templates (T2, T3, and T6) were stoichiometrically combined in 0.5 M NaCl, annealed from 64 to 4 °C, and characterized using 5% native PAGE. Discrete bands indicate the formation of DNA dendrimers, where a defined number of dendrons hybridized onto the template at near-stoichiometric ratios (Figure 1d). Using dendrons with a greater number of branches or templates with a greater number of arms yielded larger dendrimers with lower electrophoretic mobilities. To probe the sizes of these structures in 0.5 M NaCl, 10 mM phosphate buffer, dynamic light scattering (DLS) measurements were performed. 6Dn alone has a hydrodynamic diameter ( $D_{\rm h}$ ) of 5.8 nm, and the  $D_{\rm h}$ 

of the dendrimers increases with the template valency (Figure 1e). These experiments confirm that this hybridization-based synthetic approach is effective in tuning the structure of DNA-presenting building blocks.

Nanoparticle Superlattice Assembly and Crystal Structure Analysis. To synthesize colloidal crystals, DNA dendrons or dendrimers were combined with 10 nm AuNP PAEs (Figure 1b) in dendron/AuNP ratios of 16:1 or 24:1 (Table S5), selected through initial empirical observations that these ratios yield well-formed aggregates. These mixtures were then made up to 100  $\mu$ L at 0.5 M NaCl, 10 mM phosphate, and 0.015% sodium dodecyl sulfate (SDS), unless otherwise

specified (Table S6). The assemblies were heated to 60 °C, above the crystals' melting temperatures, and cooled to 22 °C at a rate of 0.1 °C per 10 min and then characterized using small-angle X-ray scattering (SAXS) in the solution state<sup>31</sup> and scanning transmission electron microscopy (STEM) in the solid state (after silica encapsulation, resin embedding, and ultramicrotomy).32 We explored the phase space using different combinations of dendrons and templates (Figure 2a and Table S5) and identified five distinct crystalline phases: face-centered cubic (FCC, Figure 2b), simple hexagonal (SH, Figure 2c), simple cubic (SC, Figure 2d), Ti<sub>S</sub>Ga<sub>4</sub>-type (Figure 2e), and graphite-type (GT, Figure 2f).<sup>33</sup> Most structures were pure and highly crystalline; however, the GT phase was always mixed with the SC phase in our system, and we also observed a partially disordered phase (Figure S3) that is structurally related to the Ti<sub>5</sub>Ga<sub>4</sub>-type phase. The Ti<sub>5</sub>Ga<sub>4</sub>-type phase is of a low space group symmetry  $(P6_3/mcm)$  and has no precedent in colloidal crystal engineering, demonstrating how the catalogue of structures possible can be expanded by using DNA dendrimers as building blocks (vide infra).

DNA dendrons (e.g., 3Dn, 4Dn, and 6Dn) were assembled with 10 nm AuNP PAEs to form colloidal crystals with FCC structures (Figure 2b). FCC crystals have been observed when AuNP PAEs were assembled with low-valent electron equivalents (EEs)<sup>34</sup> that display metallic-type colloidal bonding. Due to their low valencies, DNA dendrons function as delocalized EEs (Figure S4), bonding moieties that roam through and bind the AuNP PAE sublattice through sticky end interactions. The resulting structure is consistent with previous findings that FCC lattices are thermodynamically favorable in single-component nanoparticle systems, 35 stemming from the high symmetry and packing efficiency of the particles. A 5' TTCCTT 3' sequence was appended at the 3' end of the dendron stem in certain cases to augment dendron-AuNP PAE interactions. This sequence modification improved the crystallinities and thermostabilities of the dendron-PAE assemblies, presumably by mitigating the repulsive contributions of the long stem regions.

When two spherical PAEs with complementary sticky ends are assembled, the resulting crystal structures can be predicted using the complementary contact model (CCM).<sup>18</sup> The CCM assumes that superlattice formation maximizes the number of DNA duplexes (or "bonding") in the system. As such, crystal structures can be predicted by considering the size and linker ratios of the complementary building blocks. Thus, it is not surprising that, for 3Dn, 4Dn, and 6Dn, the crystal structure transitions from SH to SC as template valency increases (Figure 2a). SH and SC are structural equivalents of AlB<sub>2</sub> and CsCl, respectively, specifically observed when one of the two PAEs scatters X-rays to a much lesser extent, as in the case of a hollow spacer<sup>33</sup> or a DNA dendrimer (this work). However, based on the hydrodynamic diameters of the dendrimer formed from 6Dn and T6 ( $D_h$  = 14.0 nm, Figure 1e) and of the 10 nm AuNP PAE ( $D_h$  = 24.5 nm, Figure S5), and their linker ratio, the CCM predicts the formation of an SH structure, not the experimentally observed SC lattice. The reason for this deviation is discussed below.

Quantifying Superlattice Composition. We quantified the stoichiometric ratio of DNA dendrimer to AuNP in the superlattices to understand how DNA dendrimers direct nanoparticle assembly,<sup>36</sup> especially in the case of the aforementioned SC phase, which is an apparent departure from the CCM.<sup>18</sup> Specifically, the number of Cy3-labeled

dendrons and 10 nm AuNP PAEs incorporated into the crystals were quantified using UV—vis spectroscopy (Figure S6). When 6Dn was combined with T6 or T8, the resulting DNA dendrimers templated SC superlattices; analyzing the compositions of those crystals revealed that the DNA dendrimer to AuNP ratio is approximately 2:1. However, the SC phase should consist of two complementary PAEs of similar size in a 1:1 ratio. This finding suggests that two DNA dendrimers associate to give a discrete building block large enough in size to form an SC lattice when co-assembled with 10 nm AuNP PAEs.

Due to the presence of several hydrophobic moieties (e.g., DBCO) at the core of these dendrimers, we hypothesized that dendrimer-dendrimer association is enabled, at least in part, by hydrophobic interactions. To test our hypothesis, we synthesized a template free of hydrophobic moieties by conjugating alkynyl-appended DNA onto a polyamidoamine (PAMAM)-based octa-azide core. PAMAM is hydrophilic, and, compared to DBCOs, linear alkynes yield triazole linkages that are significantly less hydrophobic. The resulting template (denoted as T8'), which is free of hydrophobic moieties, was combined with 6Dn and assembled with AuNP PAEs to yield SH superlattices, as predicted by the CCM (Figure S7). In contrast, SC superlattices were formed when the DBCOcontaining T8 template was used, under identical assembly conditions. This result suggests that dendrimer-dendrimer association is likely mediated by hydrophobic interactions.

Micelle-Mediated Dendrimer-Dendrimer Association. We reasoned that SDS, added to the assembly buffer to enhance colloidal stability, can provide a confined, hydrophobic environment that brings together multiple dendrimers through micelle formation. Crucially, the critical micelle concentration (CMC) of SDS, in 0.5 M NaCl and at room temperature, is around 0.0094-0.015% (w/v).<sup>37-</sup> Realizing our assemblies were prepared in the presence of SDS micelles, we hypothesized the following pathway for dendrimer-dendrimer association (Figure 3a). Below the CMC of SDS, the DNA dendrimers do not associate with one another. At or just above the CMC of SDS, a small number of micelles form, and the hydrophobic moieties that define the core of the dendrimers insert into the micelles, mediating the association of two or more DNA dendrimers (see Figure S8 and Movies S1 and S2 for additional 3D models). Far above the CMC of SDS, the dendrimers are divided among many micelles, leading to less dendrimer-dendrimer association.

To test this hypothesis, we prepared assemblies by combining DNA dendrimers (6Dn and T6) with 10 nm AuNP PAEs and by adding an increasing amount of SDS (0, 0.005, 0.01, 0.02, and 0.04%) into assembly precursor solutions (Table S6). In situ SAXS characterization of the resulting crystals revealed that, at 0 and 0.005% SDS (Figure 3b, left), the CCM-predicted SH phases were formed, as dendrimerdendrimer associations do not occur in the absence of micelles. At 0.01% SDS, the SC phase was formed exclusively, suggesting that micelle-dendrimers assemble near the CMC of SDS. As the concentration of SDS was increased further, the SH phase begins to reappear, consistent with our hypothesis. We note that there was still some SC phase at 0.04% SDS, suggesting that the formation of high-valent micelle-dendrimers is promoted in high-concentration condensed states. We also characterized, using DLS, the solution hydrodynamic diameters of the DNA dendrimers as a function of SDS concentration. We observed considerable increases in  $D_h$  at

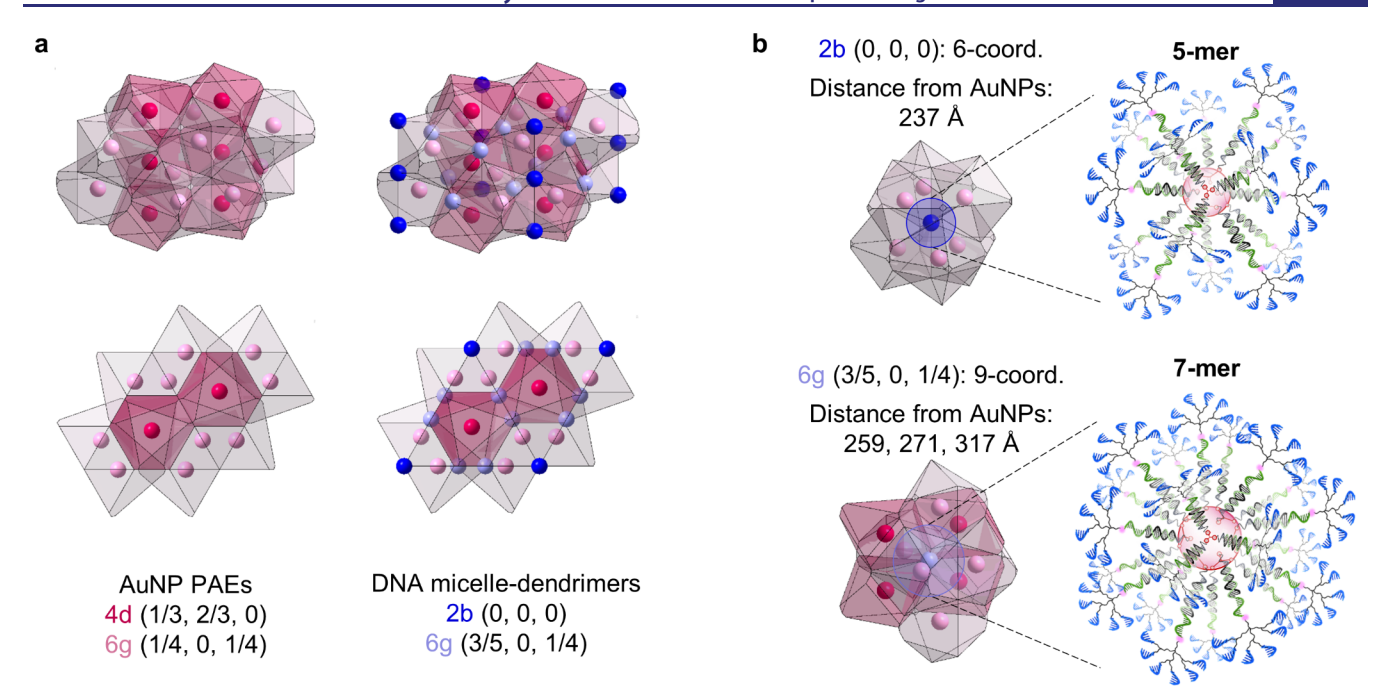


Figure 4. Structural analysis of  $Ti_5Ga_4$ -type phase. (a) Side and top-down views of a  $Ti_5Ga_4$ -type unit cell. Wyckoff positions of AuNPs are denoted by spheres in dark (4d) and pale (6g) pink. Voronoi polyhedra are constructed by considering the location of every AuNP. Within a unit cell, the polyhedra vertices meet at eight distinct locations that have the highest equidistant connectivity to the AuNPs. These are the proposed Wyckoff positions of DNA micelle-dendrimers, as denoted by the superimposed dark (0, 0, 0) and pale (3/5, 0, 1/4) blue spheres. (b) DNA micelle-dendrimers at 2b (left) are coordinated by six AuNPs at shorter distances, while those at 6g (right) are coordinated by nine AuNPs with longer distances. The significant difference in coordination environments can only be explained by the presence of micelle-dendrimers with distinct sizes and association numbers, specifically a 5-mer in 2b and a 7-mer in 6g.

0.01 and 0.02% SDS (Figure S5), consistent with our hypothesis that micelle-dendrimer formation is facilitated by a low concentration of SDS micelles. These experiments show that superlattice assembly can be guided along different pathways by controlling the degree of dendrimer—dendrimer association *via* surfactant concentration.

Understanding the Emergence of the Ti<sub>5</sub>Ga<sub>4</sub>-Type Phase. We then addressed the question of whether the micelle-dendrimer size can be changed via structure design. Specifically, we hypothesized that a longer dendron stem would place the sterically bulky branches further from the dendrimer core, allowing more dendrimers to be inserted into a single micelle without prohibitive repulsion. To test this hypothesis, we added SDS into assembly precursor solutions containing 10 nm AuNP PAEs, T3 templates, and 6Dn-L2 (long dendron stem, Figure 3b, right). SAXS revealed that, below the CMC of SDS, the SH phase was formed, as individual DNA dendrimers are only large enough to template SH lattices. At 0.01% SDS (near the CMC), when the degree of dendrimer-dendrimer association should be at its highest, the Ti<sub>5</sub>Ga<sub>4</sub>-type phase was formed. Importantly, at 0.04% SDS, when presumably there is less dendrimer-dendrimer association, the SC phase was formed exclusively. In contrast, the assemblies prepared using T3 and 6Dn (short dendron) only yielded the SH phase at 0.04% SDS (Figure S9). These results confirm our hypothesis that the dendron stem length in part determines the number of DNA dendrimers that can associate to form discrete micelle-dendrimers (Figure S10). In a similar vein, GT phases are only observed when the DNA dendrimers are made up of a long dendron (6Dn-L2 or 6Dn-L3) and a high-valent template (T6 or T8). The presence of a large micelle-dendrimer is supported by the observation that the

distances between complementary particles that are in contact are markedly longer in the GT phase than those in the SH or SC phases (Figure S11).

In the Ti<sub>5</sub>Ga<sub>4</sub>-type crystal structure, the AuNPs occupy two distinct Wyckoff positions: 4d (1/3, 2/3, 0) and 6g (1/4, 0, 1/ 4). To elucidate the locations of the DNA micelle-dendrimers, we constructed Voronoi polyhedra around the AuNPs (Figure 4a). The polyhedra vertices meet at locations that possess the highest equidistant connectivity to the AuNPs. These locations, 2b (0, 0, 0) and 6g (3/5, 0, 1/4), pinpoint the most energetically favorable sites for the micelle-dendrimers. This analysis yields two important take-aways. First, the Ti<sub>5</sub>Ga<sub>4</sub>-type phase, which has a stoichiometry of A<sub>5</sub>B<sub>4</sub> (where A is AuNP PAE and B is DNA micelle-dendrimer), resembles a class of intermetallic compounds with an archetype of Ti<sub>5</sub>Ga<sub>4</sub> (Table S7). 40,41 Second, the two Wyckoff positions for the micelle-dendrimers have distinct coordination numbers and distances from the AuNPs (Figure 4b), indicating that they are occupied by micelle-dendrimers with different sizes. These non-degenerate micelle-dendrimers can only be accessed due to the dynamic nature of micelle-mediated, dendrimerdendrimer association. Using the aforementioned quantification experiment (Figure S6), we calculated that each B site contains an average of 6.49  $\pm$  0.48 DNA dendrimers. We propose that the 2b site, with a lower coordination number and shorter distances from AuNPs, is occupied by a 5-mer, while the 6g site is occupied by a 7-mer. This averages to 6.5 DNA dendrimers per AuNP, matching the quantified composition.

The symmetry-breaking induced by these discrete micelledendrimers can also be highlighted by constructing a new set of Voronoi polyhedra around both the AuNPs and DNA micelle-dendrimers (Figure S12). Two of these Voronoi

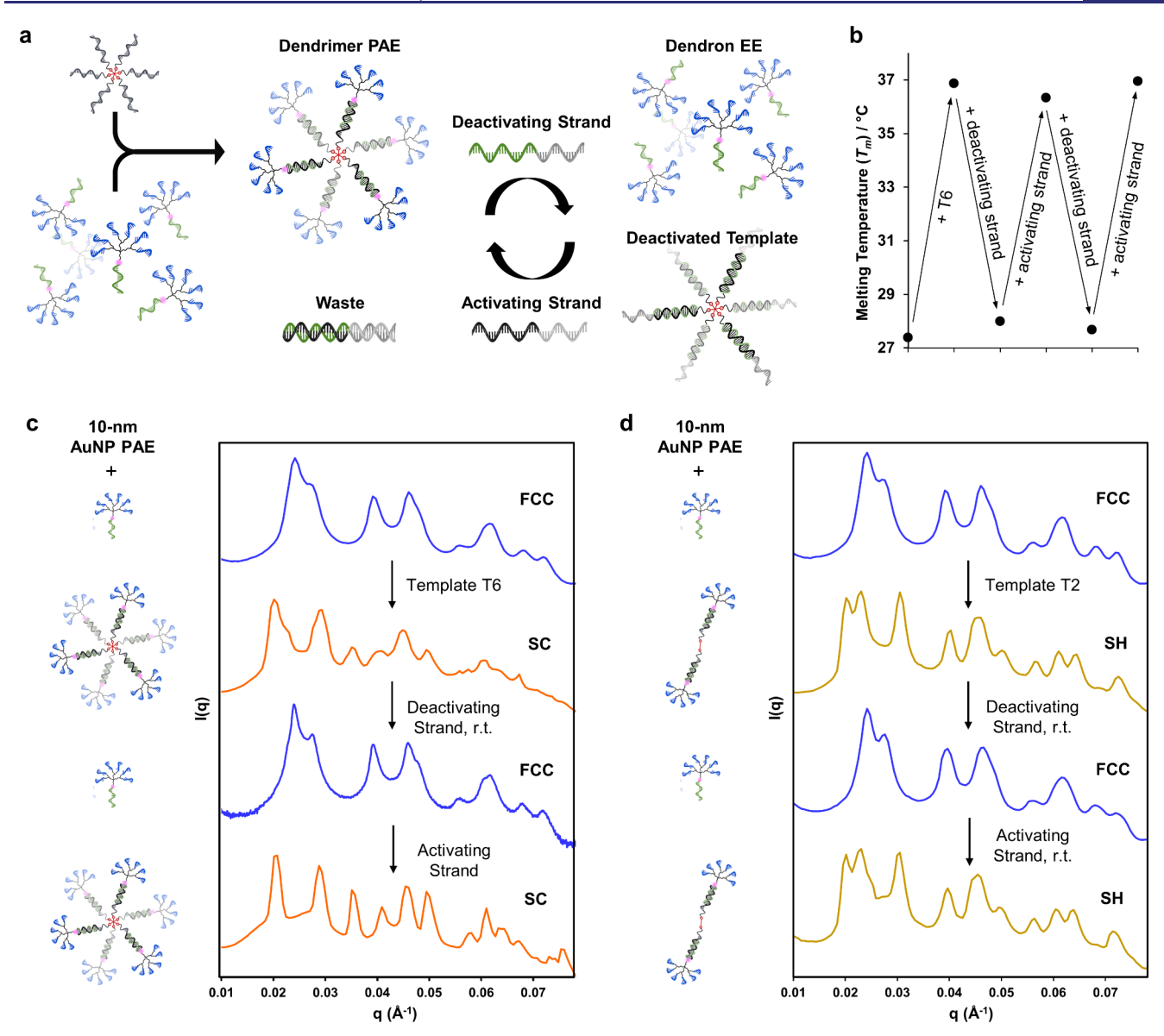


Figure 5. Colloidal crystals with switchable structures and thermostabilities. (a) Scheme outlining the design of switchable dendron/dendrimer architectures. DNA dendrons and templates can be reversibly assembled via toehold-mediated strand displacement reactions. (b) Consecutive additions of the template, the deactivating strand, and the activating strand enable one to reconfigure the thermostability of the colloidal crystal. Colloidal crystal structures were switched between FCC (blue traces) and (c) SC (orange traces) or (d) SH (yellow traces) over two full cycles in a single pot. For (d) heating and slow cooling is not required due to the diffusive nature of the DNA architectures involved, allowing the colloidal crystal structure to reorganize at room temperature.

polyhedra are Frank–Kasper (FK)-type, with a coordination number (CN) of 14, while the other two are pseudo-FK polyhedra with CNs of 13 and 17, respectively. Overall, the emergence of the Ti<sub>5</sub>Ga<sub>4</sub>-type phase is predicated on supramolecules undergoing further association, via transient interactions, into micellar architectures with discrete sizes. This type of symmetry-breaking mechanism, that is, the transition from a simple to a complex packing structure caused by the formation of unequal-sized micelles, has been observed in soft matter<sup>3,12,42</sup> but is new to systems involving inorganic nanoparticles. Thus, reorganizable supra-structures offer new routes for expanding accessible structure types in nanoparticle assembly.

Reconfigurable Crystal Structures and Bonding Character. Having explored the phase space, we set out to design stimuli-responsive crystals with reconfigurable struc-

tures and thermostabilities. To disassemble the DNA dendrimer, we designed and synthesized a linear DNA strand (deactivating strand) that is a full complement to the template and would displace the DNA dendrons from the templates via TMSD, <sup>43</sup> yielding deactivated templates and functional dendron EEs (Figure 5a). Native PAGE (Figure S13, lanes 6 and 7) showed that a slight excess of deactivating strand is required to free the dendrons completely. The key to enabling multiple cycles of structural reconfiguration is that the deactivating strand was designed with its own toehold region, such that its perfect complement (the activating strand) would remove the deactivating strand from the template via TMSD (Figure 5a). The liberated templates can combine with the dendrons to regenerate DNA dendrimers (Figure S13, lane 8), thus completing one switching cycle.

We then studied the switchability of these dendritic architectures in the context of nanoparticle superlattices to determine whether this simple DNA design can enable both the thermostability and structure to be reversibly programmed. We started by studying superlattices that were prepared using 6Dn and 10 nm AuNP PAEs. The  $T_{\rm m}$  of these crystals were characterized after the addition of a template (T6) and after consecutive additions of deactivating and activating strands. We observed changes in thermostability (Figure 5b) that follow established dependence on construct valency (Figure S4). Via in situ SAXS characterization, we confirmed that the phase symmetries change as expected (Figure 5c). When 6Dn and 10 nm AuNP PAEs were assembled, an FCC lattice was formed. Then, upon the addition of a template (T6), the dendron EEs were assembled into dendrimer PAEs, and an SC lattice was formed after thermal annealing. Subsequent addition of the deactivating strand yielded an FCC lattice after annealing at room temperature, enabled by the diffusive nature of these low-valent dendrons. Finally, after the addition of the activating strand and subsequent thermal annealing, the template rehybridized with the dendron to regenerate the DNA dendrimer, reforming an SC lattice and completing two structure switching cycles. We further took advantage of the inherent diffusivity of low-valent templates (e.g., T2) and the resulting DNA dendrimers (Figure S4) to switch crystal structures through two full cycles without having to heat or slow-cool the samples (Figure 5d). The elegance of this roomtemperature, isothermal phase symmetry reconfiguration is the simplicity of its operation and design, without having to use instruments for thermal processing, 44-47 or having to design complex DNA circuitry.4

The crystal structure reconfiguration is not limited to two structures only. By introducing a new template (e.g., T8) after a previously added template (e.g., T2) has been deactivated by the action of the block strand, we successfully traversed between an FCC, an SH, and an SC lattice in one pot (Figure S14). This type of structure reconfiguration also accommodates AuNP PAEs of different sizes. Using 5 nm AuNP PAEs, we successfully switched between an FCC lattice and an SC lattice (Figure S15). Overall, these experiments demonstrate that both the structure and the thermostability of a colloidal crystal can be reversibly altered via a simple procedure, opening avenues for designing switchable and adaptive mesoscopic materials that are templated by highly modular DNA supramolecules.

# CONCLUSIONS

This work introduces a new type of DNA-mediated hierarchical assembly that has three levels of structural organization. Importantly, the assembly outcomes cannot be rationalized, and the lattice reconfiguration strategies cannot be realized, unless all of these underlying interactions are considered. This study highlights the fact that chemical components (e.g., surfactants) or functional groups (e.g., hydrophobic moieties) that seem inconsequential can assume structure-directing roles in extended assemblies. In particular, the advances described herein should encourage re-exploration of the surfactant literature for developing new strategies to program the assembly of nanomaterials. To conclude, utilizing both sequence-encoded and non-sequence-specific interactions to mediate dynamic and reconfigurable organizations of building blocks is an effective strategy for designing hierarchical materials. These structure-guiding principles

should apply to both soft and hard matter, opening avenues for the deliberate introduction of transient interactions between building blocks to induce the formation of unconventional phases.

# ASSOCIATED CONTENT

## Supporting Information

The Supporting Information is available free of charge at https://pubs.acs.org/doi/10.1021/jacs.1c07858.

Materials and methods, assembly procedures and tables, MALDI-TOF MS data, DLS data, gel images, 3D models of DNA dendrimer and micelle-dendrimer, crystal structure analysis, SAXS data, and STEM images, including Figures S1–S28 and Tables S1–S9 (PDF) Movie S1, depicting a 3D model of a DNA dendrimer, made up of six copies of a six-branch dendron hybridized onto a six-arm template (MP4)

Movie S2, depicting a 3D model of a DNA micelledendrimer, made up of two DNA dendrimers that have their dendritic cores inserted into an SDS micelle (MP4)

#### AUTHOR INFORMATION

#### **Corresponding Author**

Chad A. Mirkin – Department of Chemistry and International Institute for Nanotechnology, Northwestern University, Evanston, Illinois 60208, United States; orcid.org/0000-0002-6634-7627; Email: chadnano@northwestern.edu

#### Authors

Ho Fung Cheng — Department of Chemistry and International Institute for Nanotechnology, Northwestern University, Evanston, Illinois 60208, United States;

orcid.org/0000-0003-2580-0912

Max E. Distler – Department of Chemistry and International Institute for Nanotechnology, Northwestern University, Evanston, Illinois 60208, United States; ⊙ orcid.org/0000-0002-3750-5075

Byeongdu Lee – X-ray Science Division, Advanced Photon Source, Argonne National Laboratory, Lemont, Illinois 60439, United States; oorcid.org/0000-0003-2514-8805

Wenjie Zhou − Department of Chemistry and International Institute for Nanotechnology, Northwestern University, Evanston, Illinois 60208, United States; orcid.org/0000-0002-7626-4032

Steven Weigand — DuPont—Northwestern—Dow Collaborative Access Team (DND-CAT) Synchrotron Research Center, Northwestern University, Argonne, Illinois 60208, United States

Complete contact information is available at: https://pubs.acs.org/10.1021/jacs.1c07858

## **Author Contributions**

<sup>‡</sup>H.F.C. and M.E.D. contributed equally.

#### Notes

The authors declare no competing financial interest.

# ACKNOWLEDGMENTS

The authors thank E. W. Roth [Northwestern University (NU)] for ultramicrotomy and X. Zuo [Argonne National Laboratory] for assistance with X-ray scattering experiments. This material is based upon work supported by the National Science Foundation grant CHE-1709888, the Air Force Office

of Scientific Research award FA9550-17-1-0348, the Sherman Fairchild Foundation, Inc., and the Air Force Research Laboratory agreement FA8650-15-2-5518. The U.S. Government is authorized to reproduce and distribute reprints for Governmental purposes notwithstanding any copyright notation thereon. The views and conclusions contained herein are those of the authors and should not be interpreted as necessarily representing the official policies or endorsements, either expressed or implied, of Air Force Research Laboratory or the U.S. Government. This work made use of the EPIC facility of Northwestern University's NUANCE Center, which has received support from the SHyNE Resource (NSF ECCS-2025633), the IIN, and Northwestern's MRSEC program (NSF DMR-1720139). This research used resources of the Advanced Photon Source (Sector 5, the DuPont-Northwestern-Dow Collaborative Access Team (DND-CAT), and the beamline 12-ID-B), a U.S. Department of Energy (DOE) Office of Science User Facility operated for the DOE Office of Science by Argonne National Laboratory under Contract No. DE-AC02-06CH11357. DND-CAT is supported by Northwestern University, The Dow Chemical Company, and DuPont de Nemours, Inc. Data collected in Sector 5 made use of an instrument funded by the National Science Foundation under Award No. 0960140.

#### REFERENCES

- (1) Matsen, M. W.; Bates, F. S. Origins of Complex Self-Assembly in Block Copolymers. *Macromolecules* **1996**, *29*, 7641–7644.
- (2) Lee, S.; Bluemle, M. J.; Bates, F. S. Discovery of a Frank-Kasper  $\sigma$  Phase in Sphere-Forming Block Copolymer Melts. *Science* **2010**, 330, 349–353.
- (3) Lee, S.; Leighton, C.; Bates, F. S. Sphericity and symmetry breaking in the formation of Frank-Kasper phases from one component materials. *Proc. Natl. Acad. Sci. U. S. A.* **2014**, *111*, 17723–17731.
- (4) Peterca, M.; Percec, V. Recasting metal alloy phases with block copolymers. *Science* **2010**, 330, 333–334.
- (\$\(\frac{5}{5}\)) Balagurusamy, V. S. K.; Ungar, G.; Percec, V.; Johansson, G. Rational Design of the First Spherical Supramolecular Dendrimers Self-Organized in a Novel Thermotropic Cubic Liquid-Crystalline Phase and the Determination of Their Shape by X-ray Analysis. *J. Am. Chem. Soc.* **1997**, *119*, 1539–1555.
- (6) Ungar, G.; Liu, Y.; Zeng, X.; Percec, V.; Cho, W.-D. Giant Supramolecular Liquid Crystal Lattice. *Science* **2003**, 299, 1208–1211.
- (7) Rosen, B. M.; Wilson, C. J.; Wilson, D. A.; Peterca, M.; Imam, M. R.; Percec, V. Dendron-Mediated Self-Assembly, Disassembly, and Self-Organization of Complex Systems. *Chem. Rev.* **2009**, *109*, 6275–6540.
- (8) Sun, H.-J.; Zhang, S.; Percec, V. From structure to function via complex supramolecular dendrimer systems. *Chem. Soc. Rev.* **2015**, *44*, 3900–3923.
- (9) Yu, X.-F.; Zhong, S.; Li, X.-P.; Tu, Y.-F.; Yang, S.-G.; Van Horn, R. M.; Ni, C.-Y.; Pochan, D. J.; Quirk, R. P.; Wesdemiotis, C.; Zhang, W.-B.; Cheng, S. Z. D. A Giant Surfactant of Polystyrene-(Carboxylic Acid-Functionalized Polyhedral Oligomeric Silsesquioxane) Amphiphile with Highly Stretched Polystyrene Tails in Micellar Assemblies. *J. Am. Chem. Soc.* **2010**, *132*, 16741–16744.
- (10) Huang, M.; Hsu, C.-H.; Wang, J.; Mei, S.; Dong, X.; Li, Y.; Li, M.; Liu, H.; Zhang, W.; Aida, T.; Zhang, W.-B.; Yue, K.; Cheng, S. Z. D. Selective assemblies of giant tetrahedra via precisely controlled positional interactions. *Science* **2015**, *348*, 424–428.
- (11) Yue, K.; Huang, M.; Marson, R. L.; He, J.; Huang, J.; Zhou, Z.; Wang, J.; Liu, C.; Yan, X.; Wu, K.; Guo, Z.; Liu, H.; Zhang, W.; Ni, P.; Wesdemiotis, C.; Zhang, W.-B.; Glotzer, S. C.; Cheng, S. Z. D. Geometry induced sequence of nanoscale Frank-Kasper and

- quasicrystal mesophases in giant surfactants. *Proc. Natl. Acad. Sci. U. S. A.* **2016**, *113*, 14195–14200.
- (12) Su, Z.; Hsu, C.-H.; Gong, Z.; Feng, X.; Huang, J.; Zhang, R.; Wang, Y.; Mao, J.; Wesdemiotis, C.; Li, T.; Seifert, S.; Zhang, W.; Aida, T.; Huang, M.; Cheng, S. Z. D. Identification of a Frank-Kasper Z phase from shape amphiphile self-assembly. *Nat. Chem.* **2019**, *11*, 899–905.
- (13) Shenhar, R.; Norsten, T. B.; Rotello, V. M. Polymer-mediated nanoparticle assembly: structural control and applications. *Adv. Mater.* **2005**, *17*, 657–669.
- (14) Wang, Y.; Desroches, G. J.; Macfarlane, R. J. Ordered polymer composite materials: challenges and opportunities. *Nanoscale* **2021**, 13, 426–443.
- (15) Mirkin, C. A.; Letsinger, R. L.; Mucic, R. C.; Storhoff, J. J. A DNA-based method for rationally assembling nanoparticles into macroscopic materials. *Nature* **1996**, 382, 607–609.
- (16) Park, S. Y.; Lytton-Jean, A. K. R.; Lee, B.; Weigand, S.; Schatz, G. C.; Mirkin, C. A. DNA-programmable nanoparticle crystallization. *Nature* **2008**, *451*, 553–556.
- (17) Nykypanchuk, D.; Maye, M. M.; van der Lelie, D.; Gang, O. DNA-guided crystallization of colloidal nanoparticles. *Nature* **2008**, 451, 549–552.
- (18) Macfarlane, R. J.; Lee, B.; Jones, M. R.; Harris, N.; Schatz, G. C.; Mirkin, C. A. Nanoparticle Superlattice Engineering with DNA. *Science* **2011**, 334, 204–208.
- (19) Macfarlane, R. J.; O'Brien, M. N.; Petrosko, S. H.; Mirkin, C. A. Nucleic Acid-Modified Nanostructures as Programmable Atom Equivalents: Forging a New "Table of Elements". *Angew. Chem., Int. Ed.* **2013**, *52*, 5688–5698.
- (20) Nilsen, T. W.; Grayzel, J.; Prensky, W. Dendritic nucleic acid structures. *J. Theor. Biol.* **1997**, *187*, 273–284.
- (21) Li, Y.; Tseng, Y. D.; Kwon, S. Y.; d'Espaux, L.; Bunch, J. S.; McEuen, P. L.; Luo, D. Controlled assembly of dendrimer-like DNA. *Nat. Mater.* **2004**, *3*, 38–42.
- (22) Li, Y.; Cu, Y. T. H.; Luo, D. Multiplexed detection of pathogen DNA with DNA-based fluorescence nanobarcodes. *Nat. Biotechnol.* **2005**, 23, 885–889.
- (23) Lee, J. B.; Roh, Y. H.; Um, S. H.; Funabashi, H.; Cheng, W.; Cha, J. J.; Kiatwuthinon, P.; Muller, D. A.; Luo, D. Multifunctional nanoarchitectures from DNA-based ABC monomers. *Nat. Nanotechnol.* **2009**, *4*, 430–436.
- (24) Rattanakiat, S.; Nishikawa, M.; Funabashi, H.; Luo, D.; Takakura, Y. The assembly of a short linear natural cytosine-phosphate-guanine DNA into dendritic structures and its effect on immunostimulatory activity. *Biomaterials* **2009**, *30*, 5701–5706.
- (25) Lu, J.; Hu, P.; Cao, L.; Wei, Z.; Xiao, F.; Chen, Z.; Li, Y.; Tian, L. Genetically Encoded and Biologically Produced All-DNA Nanomedicine Based on One-Pot Assembly of DNA Dendrimers for Targeted Gene Regulation. *Angew. Chem., Int. Ed.* **2021**, *60*, 5377–5385.
- (26) Thaner, R. V.; Eryazici, I.; Farha, O. K.; Mirkin, C. A.; Nguyen, S. B. T. Facile one-step solid-phase synthesis of multi-topic organic-DNA hybrids via "click" chemistry. *Chem. Sci.* **2014**, *5*, 1091–1096.
- (27) Cheng, H. F.; Wang, S.; Mirkin, C. A. Electron-Equivalent Valency through Molecularly Well-Defined Multivalent DNA. *J. Am. Chem. Soc.* **2021**, *143*, 1752–1757.
- (28) Shchepinov, M. S.; Udalova, I. A.; Bridgman, A. J.; Southern, E. M. Oligonucleotide dendrimers: synthesis and use as polylabelled DNA probes. *Nucleic Acids Res.* **1997**, *25*, 4447–4454.
- (29) Shchepinov, M. S.; Mir, K. U.; Elder, J. K.; Frank-Kamenetskii, M. D.; Southern, E. M. Oligonucleotide dendrimers: stable nanostructures. *Nucleic Acids Res.* **1999**, *27*, 3035–3041.
- (30) Distler, M. E.; Teplensky, M. H.; Bujold, K. E.; Kusmierz, C. D.; Evangelopoulos, M.; Mirkin, C. A. DNA Dendrons as Agents for Intracellular Delivery. *J. Am. Chem. Soc.* **2021**, *143*, 13513–13518.
- (31) Li, T.; Senesi, A. J.; Lee, B. Small Angle X-ray Scattering for Nanoparticle Research. *Chem. Rev.* **2016**, *116*, 11128–11180.
- (32) Auyeung, E.; Macfarlane, R. J.; Choi, C. H. J.; Cutler, J. I.; Mirkin, C. A. Transitioning DNA-Engineered Nanoparticle Super-

lattices from Solution to the Solid State. Adv. Mater. 2012, 24, 5181–5186.

- (33) Auyeung, E.; Cutler, J. I.; Macfarlane, R. J.; Jones, M. R.; Wu, J.; Liu, G.; Zhang, K.; Osberg, K. D.; Mirkin, C. A. Synthetically programmable nanoparticle superlattices using a hollow three-dimensional spacer approach. *Nat. Nanotechnol.* **2012**, *7*, 24–28.
- (34) Girard, M.; Wang, S.; Du, J. S.; Das, A.; Huang, Z.; Dravid, V. P.; Mirkin, C. A.; Olvera de la Cruz, M. Particle analogs of electrons in colloidal crystals. *Science* **2019**, *364*, 1174–1178.
- (35) Whetten, R. L.; Shafigullin, M. N.; Khoury, J. T.; Schaaff, T. G.; Vezmar, I.; Alvarez, M. M.; Wilkinson, A. Crystal Structures of Molecular Gold Nanocrystal Arrays. *Acc. Chem. Res.* **1999**, 32, 397–406.
- (36) Wang, M. X.; Brodin, J. D.; Millan, J. A.; Seo, S. E.; Girard, M.; Olvera de la Cruz, M.; Lee, B.; Mirkin, C. A. Altering DNA-Programmable Colloidal Crystallization Paths by Modulating Particle Repulsion. *Nano Lett.* **2017**, *17*, 5126–5132.
- (37) Emerson, M. F.; Holtzer, A. On the ionic strength dependence of micelle number. II. *J. Phys. Chem.* **1967**, *71*, 1898–1907.
- (38) Hayashi, S.; Ikeda, S. Micelle size and shape of sodium dodecyl sulfate in concentrated sodium chloride solutions. *J. Phys. Chem.* **1980**, *84*, 744–751.
- (39) Stellner, K. L.; Scamehorn, J. F. Hardness tolerance of anionic surfactant solutions. 1. Anionic surfactant with added monovalent electrolyte. *Langmuir* 1989, 5, 70–77.
- (40) Schubert, K.; Meissner, H. G.; Poetzschke, M.; Rossteutscher, W.; Stolz, E. Structure data on metallic phases. VII. *Naturwissenschaften* **1962**, *49*, 57.
- (41) Rieger, W.; Nowotny, H.; Benesovsky, F. Phases with octahedral units of transition metals. *Monatsh. Chem.* **1965**, *96*, 232–241.
- (42) Kim, S. A.; Jeong, K.-J.; Yethiraj, A.; Mahanthappa, M. K. Low-symmetry sphere packings of simple surfactant micelles induced by ionic sphericity. *Proc. Natl. Acad. Sci. U. S. A.* **2017**, *114*, 4072–4077.
- (43) Zhang, D. Y.; Seelig, G. Dynamic DNA nanotechnology using strand-displacement reactions. *Nat. Chem.* **2011**, *3*, 103–113.
- (44) Zhang, Y.; Pal, S.; Srinivasan, B.; Vo, T.; Kumar, S.; Gang, O. Selective transformations between nanoparticle superlattices via the reprogramming of DNA-mediated interactions. *Nat. Mater.* **2015**, *14*, 840–847.
- (45) Kim, Y.; Macfarlane, R. J.; Jones, M. R.; Mirkin, C. A. Transmutable nanoparticles with reconfigurable surface ligands. *Science* **2016**, *351*, 579–582.
- (46) Zhu, J.; Kim, Y.; Lin, H.; Wang, S.; Mirkin, C. A. pH-Responsive Nanoparticle Superlattices with Tunable DNA Bonds. *J. Am. Chem. Soc.* **2018**, *140*, 5061–5064.
- (47) Oh, J. S.; Yi, G.-R.; Pine, D. J. Reconfigurable Self-Assembly and Kinetic Control of Multiprogrammed DNA-Coated Particles. *ACS Nano* **2020**, *14*, 4595–4600.
- (48) Zhou, X.; Yao, D.; Hua, W.; Huang, N.; Chen, X.; Li, L.; He, M.; Zhang, Y.; Guo, Y.; Xiao, S.; Bian, F.; Liang, H. Programming colloidal bonding using DNA strand-displacement circuitry. *Proc. Natl. Acad. Sci. U. S. A.* **2020**, *117*, 5617–5623.